

# Optical Engineering

[SPIDigitalLibrary.org/oe](http://SPIDigitalLibrary.org/oe)

## **Broadband compact reflector based on all-dielectric subwavelength nanoparticle chains: reflecting lights beyond normal incidence with a very high reflectivity**

Hao Li  
Wei Li  
Aimin Wu  
Chao Qiu  
Zhen Sheng  
Xi Wang  
Shichang Zou  
Fuwan Gan

# Broadband compact reflector based on all-dielectric subwavelength nanoparticle chains: reflecting lights beyond normal incidence with a very high reflectivity

**Hao Li**

Chinese Academy of Sciences  
Shanghai Institute of Microsystem and Information  
Technology  
State Key Laboratory of Functional Materials for  
Informatics  
Shanghai 200050, China  
and  
University of Chinese Academy of Sciences  
Beijing 100049, China  
E-mail: [lihao@mail.sim.ac.cn](mailto:lihao@mail.sim.ac.cn)

**Wei Li**

**Aimin Wu**

**Chao Qiu**

**Zhen Sheng**

**Xi Wang**

**Shichang Zou**

**Fuwan Gan**

Chinese Academy of Sciences  
Shanghai Institute of Microsystem and Information  
Technology  
State Key Laboratory of Functional Materials for  
Informatics  
Shanghai 200050, China

**Abstract.** We report a polarization-dependent reflector beyond normal incidence with a subwavelength nanoparticle chain. Polarization-dependent reflection with high reflectivity or high transmissivity can be obtained with this structure. Light waves of transverse electric/magnetic mode will be reflected, while the transverse magnetic/electric mode will transmit through. The structure shows a certain degree of tolerance of incident angle, technical fabrication, and even particle shape. We hope the low-loss and compact structure can find applications in photonic circuits such as gallium nitride-based light sources. © The Authors. Published by SPIE under a Creative Commons Attribution 3.0 Unported License. Distribution or reproduction of this work in whole or in part requires full attribution of the original publication, including its DOI. [DOI: [10.1117/1.OE.52.6.068001](https://doi.org/10.1117/1.OE.52.6.068001)]

Subject terms: reflector; subwavelength; nanostructure.

Paper 130455 received Mar. 22, 2013; revised manuscript received May 6, 2013; accepted for publication May 7, 2013; published online Jun. 3, 2013.

## 1 Introduction

As one of the most prevalent optical devices, reflectors are widely used in imaging, solar energy collection, laser cavities, etc. Traditionally, metallic mirrors are used to reflect light over a broad range of frequencies. However, in the infrared and visible light region, losses from mirrors are inevitable and may severely limit the performance of reflector-based devices. To avoid metallic losses, much effort has been devoted to the area of total or anomalous reflection based on all-dielectric structures, such as conventional distributed Bragg reflectors, bandgap-based photonic crystal,<sup>1-4</sup> and resonant gratings.<sup>5</sup> However, they suffer from issues of scale (too large), due to periodicity, or frequency (too narrow), due to the resonance effect.

Recently, a new ultra-compact structure (i.e., an all-dielectric subwavelength-particle chain) has offered another option for light control. The properties of the structure have found many applications in physics and engineering, including light energy transfer,<sup>6,7</sup> light generation,<sup>8-13</sup> negative transmission,<sup>14</sup> optical sensing and detecting,<sup>15</sup> and nonlinear optics.<sup>16</sup> These works provide us deep insight into the extraordinary scattering properties of the nanoparticle chain.

Based on the all-dielectric subwavelength-nanoparticle chain, in this paper, we propose an alternative design for a reflector without any metallic losses. Numerical methods such as finite-difference time-domain<sup>17</sup> or finite element method can be used for numerical results for the reflector. But for the underlying physics, theoretical analysis is

necessary. Multiple scattering theories are widely used for the calculation of nanoparticles.<sup>14,18</sup> However, they are limited to circular particles. In this work, a simple analytic analysis is used for a reflector composed of square nanoparticles. We show that our ultra-compact, broadband reflector can totally reflect polarized light beyond the normal incidence. Our device has also great potential as a compact on-chip polarizer for separating two linearly polarized light beams by reflecting one polarized beam and transmitting the other.

Obviously, our design can be widely used in optical devices. To show this with a typical example, we choose an all dielectric nanoparticle-based reflector made of gallium nitride (GaN) working in the blue light region (with a wavelength of about 450 to 495 nm). The reflector can be used to enhance the performance of GaN-based optical devices such as GaN light-emitting diodes (LEDs), due to its high reflection and material matching.<sup>19</sup> Finally, we provide the principles and guidance for designing such devices, which are not limited to GaN-based optical devices.

## 2 Theoretical Analysis

The theoretical analysis of high-contrast grating with the nanoparticles of a square cross-section will be applied to the particle array with low-contrast index material.<sup>12,13,20</sup> The schematic of the structure of a square cross-section is presented in Fig. 1. The incident plane is  $z = -t_g$ , and the out plane is  $z = 0$ . An array of particles are arranged along the  $x$ -direction, with a separation between adjacent

particles of  $T = 400$  nm. Here we consider the two-dimensional (2-D) case. The structure is uniform and infinite along the  $y$ -direction, and the chain is infinite along the  $x$ -direction. In practical applications, a structure with an infinite length is impossible. But the structure can be fabricated so long (tens of microns, which is much larger than the incident wavelength)<sup>12,13</sup> in the  $y$ -direction and the  $x$ -direction that the 2-D calculation will also provide an approximate result. The nanoparticles are made of GaN with low indices of about  $n_{\text{GaN}} = 2.5$  in the blue light region, and the surrounding medium is assumed to be air ( $n_{\text{air}} = 1$ ). The side length of the square particle is  $t_g = 227$  nm. For simplicity, we consider the transverse electric (TE) polarized normal incidence with the  $H$  field along the axis of particles ( $y$ -direction).

In the reflection region ( $z \leq -t_g$ ), the magnetic field distribution  $H_y$  can be expressed as

$$H_y = \exp[-j(2\pi/\lambda)(z + t_g)] - \sum_{n=0}^{\infty} r_n h_{y,n}^{\text{out}}(x) \{ \exp[+j\gamma_n(z + t_g)] \}. \quad (1)$$

In the grating region ( $-t_g < z < 0$ ),  $H_y$  can be expressed as

$$H_y = \sum_{m=1}^{\infty} h_{y,m}^{\text{in}}(x) [a_m \exp(-j\beta_m z) - a_m^p \exp(+j\beta_m z)]. \quad (2)$$

And in the transmission region ( $z \geq 0$ ),  $H_y$  can be expressed as

$$H_y = \sum_{n=0}^{\infty} \tau_n h_{y,n}^{\text{out}}(x) [\exp(+j\gamma_n z)], \quad (3)$$

where  $m = 1, 2, \dots$  denotes the number of the grating mode;  $n = 0, 1, \dots$  denotes the number of the reflect or transmit mode;  $\beta_m$  and  $\gamma_n$  are the longitudinal wave number in and outside the grating region, respectively;  $r_n$  and  $\tau_n$  are the coefficients of the reflected and transmitted modes, respectively;  $h_{y,m}^{\text{in}}$  and  $h_{y,m}^{\text{out}}$  are the lateral field profile in and outside the grating, respectively; and  $a_m$  and  $a_m^p$  are the coefficients of the forward and backward propagating components, respectively.

In the grating region, along the  $z$ -direction, the grating can be seen as a periodic slab waveguide. By matching the boundary conditions along  $x = 0$  and  $x = a$ , the dispersion relation between the lateral wave numbers  $k_a$  and  $k_s$  inside air-gaps and GaN particles can be obtained as

$$n_{\text{GaN}}^{-2} k_{s,m} \tan(k_{s,m} t_g / 2) = -k_{a,m} \tan(k_{a,m} a / 2), \quad (4)$$

where  $\beta_m^2 = (2\pi/\lambda)^2 - k_{a,m}^2 = (2\pi n_{\text{GaN}}/\lambda)^2 - k_{s,m}^2$ .

Finally, by matching the boundary conditions at  $z = 0$  and  $z = -t_g$ , the field distribution in the whole region can be solved. Due to the principle of duality of TE and transverse magnetic (TM) waves, the field distribution for another polarization can also be obtained as described above.

It is worth mentioning that, for a subwavelength structure ( $T < \lambda$ ), the reflectivity or transmissivity totally depends on the zeroth-order diffraction  $\tau_0$ , since the longitudinal wave number is determined by  $\gamma_n^2 = (2\pi/\lambda)^2 - (2n\pi/T)^2$ , and one can find that only the zeroth-order diffraction is propagating, and higher orders are all evanescent. Therefore, we

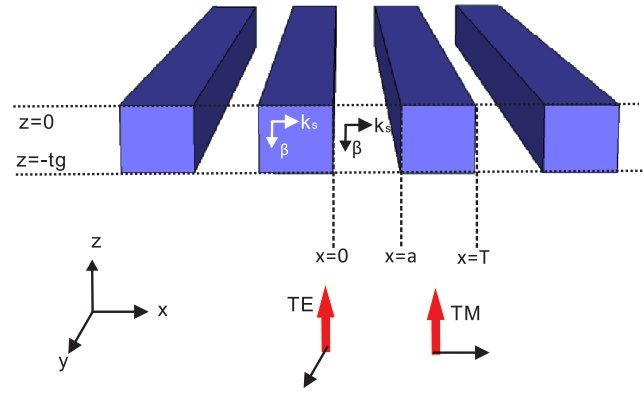


**Fig. 1** Schematic of the nanoparticle chain with a square cross-section. The incident plane is  $z = -t_g$ , and the out plane is  $z = 0$ . The parameters for this plot are  $T = 400$  nm,  $t_g = 227$  nm. The red arrow indicates the direction of wave incidence. The black arrows correspond to the  $H$ -field direction in both TE and TM polarizations of incidence.

can achieve high reflectivity or transmissivity by controlling  $\tau_0$ , which is given as

$$\tau_0 = \sum_{m=1}^{\infty} (a_m - a_m^p) T^{-1} \int_0^T h_{y,m}^{\text{in}}(x) dx. \quad (5)$$

### 3 Results and Discussion

In Fig. 2(a), the  $H$  field intensity pattern of the TE mode at wavelength  $\lambda = 480$  nm is presented. One can notice that most of the light waves toward the  $z$ -direction are reflected back by the layer of nanoparticles. In the top panel of Fig. 2(b), we present the reflectivity for the TE mode with the solid blue line in the blue light region. For comparison, the reflectivity of typical Ag film is presented with the solid green line. The optical constants of silver are from Palik.<sup>21</sup> At the wavelength  $\lambda = 460$  nm, the complex index of Ag is  $n = 0.144 + 2.56i$ . In practical applications, GaN-based LEDs are widely used, but the light extraction efficiency (LEE) is not sufficient, because of the trapping of light inside the semiconductor.<sup>19</sup> One method to improve the LEE is depositing silver film on the bottom of the LED. The reflection of silver film results in more light being extracted from the top of the device. However, due to the metallic material absorption loss, the reflectivity of typical Ag film is no more than 95%. But with the particle array, we can get obviously higher reflectivity with the same semiconductor material. On the other hand, we get almost the opposite reflection effect for other polarized waves, as shown in the bottom panel of Fig. 2(b). The TM mode waves are completely separated from the TE modes, and the reflectivity is no more than 1% from 460 to 490 nm. The discrepant reflectivity for different polarized waves shows the potential application for polarization suppression in light sources.

For the underlying physics of the reflection phenomenon, we present the first three grating modes for TE waves in Fig. 3(a)–3(c). The dispersion relation in Eq. (4) determines the profile of grating modes in the form of  $\beta_m$ . The mode profiles (propagating mode or evanescent mode along the  $z$ -direction) depend on whether the value of  $\beta_m$  is real or imaginary. In this case, we found only the first two modes are existing in the grating, while the other modes

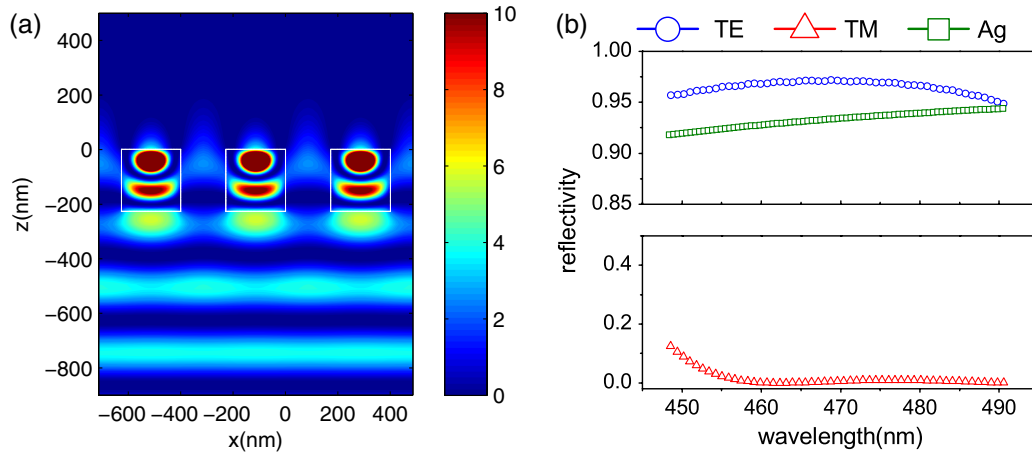


**Fig. 2** (a) Distribution of  $H$  field intensity when a TE mode plane wave strikes an array of nanoparticles in the  $x$ -direction with a side length  $t_g = 227$  nm. The particles are marked with a white solid line. (b) Reflectivity in the blue light region. The blue, red, green lines correspond to the TE waves, the TM waves, and typical Ag film, respectively.

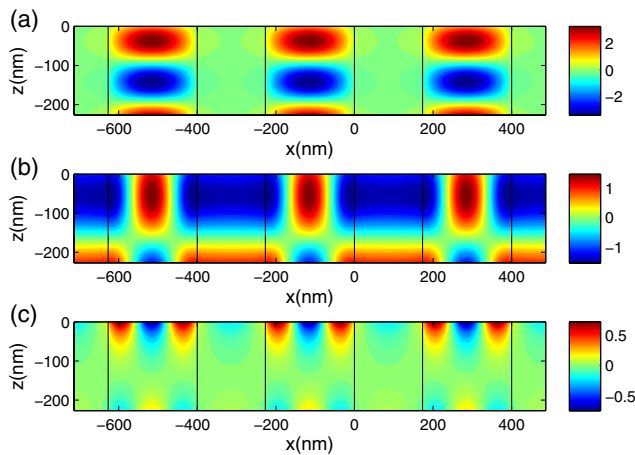


**Fig. 3** The contour of  $H_y$  field distribution of the first three grating modes. The grating bars are marked by solid squares. The first two modes (a) and (b) are propagating modes in the grating, and the third mode (c) is the evanescent mode. This means that  $\beta_1$  and  $\beta_2$  are real, while  $\beta_3, \dots$  are imaginary.

are cut off ( $\beta_1$  and  $\beta_2$  are real, but  $\beta_3, \dots$  are imaginary). It is easy to notice in Fig. 3(c) that the field decays along the  $z$ -direction, which is in agreement with the imaginary wave number. The superposition of these grating modes in the form of Eq. (5) finally results in the transmission field. Actually, for a high reflectivity range, the first two modes are enough<sup>20</sup> for the convergence of the solution of  $\tau_0$ . Therefore, the reflection with a high reflectivity or transmission with a high transmissivity can be seen as a result of destructive or constructive interference of the grating modes.

In most real cases, reflection with a high reflectivity for normal incidence should not be obtained. For our structure, the polarization-dependent reflection phenomenon is not limited to the normal incidence case. We then consider the oblique incidence case with a small incident angle. The reflectivity contours versus the wavelength and incident angle for both TE modes and TM mode are presented in Fig. 4(a) and 4(b). The working range for our structure is marked with the black arrows, corresponding to the reflection with a high reflectivity and the transmission with a high transmissivity,

respectively. Figure 4(c) shows the reflectivity with an incident angle from  $-10$  to  $10$  deg at a wavelength of  $480$  nm. The results illustrate that, even for the oblique incidence, high reflectivity and good polarization control can be obtained, providing a certain degree of angular tolerance for the reflector.

To give a clear design principle, we consider a structure a period  $T = 400$  nm. The reflectivity contours versus the side length of the square and the wavelength are presented in Fig. 5. The TE mode and TM mode correspond to (a) and (b), respectively. We focus on the reflection region with a high reflectivity or transmission region with a high transmissivity for both modes, and the overlap region will be valuable for specific applications. In our case, we choose region A (marked with the white arrow) to achieve a broadband reflection in Fig. 5(a), while a deep transmission for the TM mode is shown in the corresponding region of Fig. 5(b). Likewise, in region B, the TE waves will pass through, while the TM waves are reflected back. Similarly, we can achieve reflection with a high reflectivity or transmission with a high transmissivity for both modes by choosing the working region appropriately. In addition, we can observe a clear boundary at the wavelength  $\lambda = 400$  nm. The broadband reflection regions with a high reflectivity or the transmission regions with a high transmissivity are mainly distributed above the boundary. The field distribution of different diffraction orders in the transmission region is given by Eq. (3). In this case (normal incidence), for a subwavelength structure ( $\lambda > T$ ), only the zeroth diffraction order is propagating ( $\gamma_0$  is real), while the first, second, and higher orders are all evanescent ( $\gamma_0, \gamma_1, \dots$  are imaginary). High reflectivity can be achieved in such a structure by merely suppressing the zeroth transmissive diffraction order (i.e.,  $\tau_0 = 0$ ). Had there been more than one transmitted and reflected diffraction order (i.e., when  $\lambda < T$ ), obtaining high reflectivity through the cancellation of multiple orders ( $\tau_0 = 0, \tau_1 = 0, \tau_2 = 0, \dots$ ) would be very difficult. Therefore, high reflectivity can be easily achieved, because, for a subwavelength structure, only the zeroth-order diffraction needs to be suppressed, while the ordinary structure will result in many higher-order diffractions. The boundary in Fig. 5(a) and 5(b) at a wavelength of  $\lambda = 400$  nm can be seen as the dividing

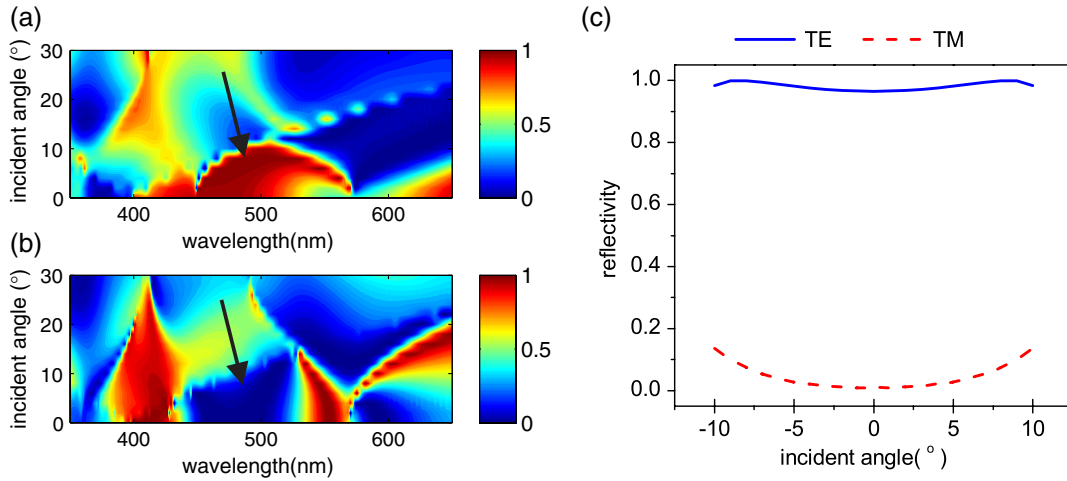


**Fig. 4** The reflectivity contours versus the wavelength and incident angle for (a) the TE mode and (b) the TM mode. (c) Reflectivity in a oblique incidence case with an incident angle from  $-10$  to  $10$  deg at a wavelength of  $480$  nm.

line between a subwavelength structure and an ordinary structure.

In practical applications, due to the imperfection of the fabrication technology or other factors, a certain degree of size tolerance is necessary. We then turn our attention to the tolerance of the structure. Figure 5(c) shows the direct variation tendency of reflectivity with increasing side length.

One can notice that, for both the TE and TM modes, as the nanoparticles increase in size, the working wavelength moves toward the long wavelength direction. But the broadband property gives this structure a certain degree of immunity to the wavelength movement. Assuming the working wavelength is  $\lambda = 480$  nm, the fabrication tolerance can be at least  $10$  nm, according to Fig. 5(c).

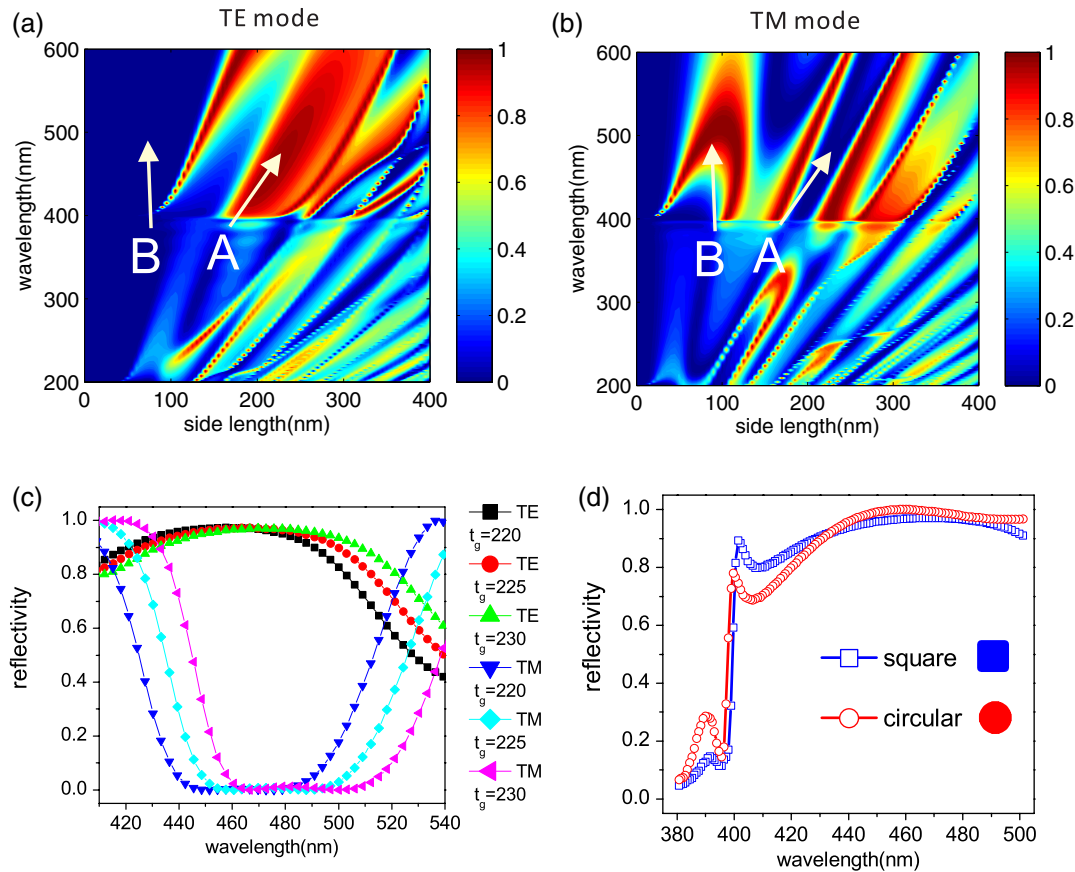


**Fig. 5** The reflectivity contours versus the side length of the square and the frequency for both (a) TE mode and (b) TM mode. (c) Reflectivity for TE and TM mode light with different size square particles. The side length of the particles are  $220$ ,  $225$ , and  $230$  nm, respectively. (d) Reflectivity versus wavelength for square and circular nanoparticle chains, corresponding to the solid blue and red lines, respectively. The radius of the circular rod is  $r = 128$  nm.

Finally, we found the phenomenon is not limited to the shape of the particle. Nanoparticles with a square cross-section can even be replaced by those with a circular cross-section with a similar reflection property, as shown in Fig. 5(d). The radius of the circular rod is chosen to be  $r = 128$  nm for equal area to the square particle. The reflectivity of the circular rod structure is calculated by using multiple scattering theory.<sup>14,18</sup> The high reflectivity is believed to be due to the same underlying physics. Since both types of structure work well, we can choose a circular or square cross-section for convenience in practical applications.

#### 4 Conclusion

In this work, we have shown a wide-band, polarization-dependent reflector beyond normal incidence with a subwavelength nanoparticle chain. In comparison with previous work, this structure offers an acceptable tolerance of incident angle, technical fabrication, and even particle shape. Because of the compact characteristic and lossless material operating in the optical frequency, it may provide us an alternate way to design the optical components in photonic circuits.

#### Acknowledgments

This research was sponsored by the Natural Science Foundation of China (Grant Nos. 61107031, 11104305, 11204340, and 61275112), the 863 Project (Grant No. 2012AA012202), and the Science and Technology Commission of Shanghai Municipality (Grant Nos. 10DJ1400400, 11ZR1443700, and 11ZR1443800).

#### References

1. D. Maystre, "Photonic crystal diffraction gratings," *Opt. Express* **8**(3), 209–216 (2001).
2. V. Mocella et al., "Influence of surface termination on negative reflection by photonic crystals," *Opt. Express* **15**(11), 6605–6611 (2007).
3. V. Lousse et al., "Angular and polarization properties of a photonic crystal slab mirror," *Opt. Express* **12**(8), 1575–1582 (2004).
4. S. Boutami et al., "Broadband and compact 2-d photonic crystal reflectors with controllable polarization dependence," *IEEE Photon. Tech. Lett.* **18**(7), 835–837 (2006).
5. S. Peng and G. M. Morris, "Experimental demonstration of resonant anomalies in diffraction from two-dimensional gratings," *Opt. Lett.* **21**(8), 549–551 (1996).
6. A. Yariv et al., "Coupled-resonator optical waveguide: a proposal and analysis," *Opt. Lett.* **24**(11), 711–713 (1999).
7. J. Du et al., "Guiding electromagnetic energy below the diffraction limit with dielectric particle arrays," *Phys. Rev. A* **79**(5), 051801 (2009).
8. K. I. Mazzitello et al., "Electrically driven light emission from an array of Si nanoclusters," *J. Phys. D Appl. Phys.* **37**(5), 668–673 (2004).
9. M. Laroche et al., "Optical resonances in one-dimensional dielectric nanorod arrays: field-induced fluorescence enhancement," *Opt. Lett.* **32**(18), 2762–2764 (2007).
10. V. O. Byelobrov et al., "Low-threshold lasing eigenmodes of an infinite periodic chain of quantum wires," *Opt. Lett.* **35**(21), 3634–3636 (2010).
11. A. K. Tiwari et al., "Collective lasing from a linear array of dielectric microspheres with gain," *Opt. Express* **20**(6), 6598–6603 (2012).
12. M. C. Huang, Y. Zhou, and C. J. Chang-Hasnain, "A surface-emitting laser incorporating a high-index-contrast subwavelength grating," *Nat. Photon.* **1**(2), 119–122 (2007).
13. M. C. Huang, Y. Zhou, and C. J. Chang-Hasnain, "Polarization mode control in high contrast subwavelength grating vcsel," presented at *Conf. on Lasers and Electro-Optics/Quantum Electronics and Laser Science Conference and Photonic Applications Systems Technologies*, OSA, San Jose, CA (2008).
14. J. Du et al., "Optical beam steering based on the symmetry of resonant modes of nanoparticles," *Phys. Rev. Lett.* **106**(20), 203903 (2011).
15. S. V. Boriskina and B. M. Reinhard, "Adaptive on-chip control of nano-optical fields with optoplasmonic vortex nanogates," *Opt. Express* **19**(22), 22305–22315 (2011).
16. D. C. Marinica, A. G. Borisov, and S. V. Shabanov, "Second harmonic generation from arrays of subwavelength cylinders," *Phys. Rev. B* **76**(8), 085311 (2007).
17. W. Li et al., "Switchable hyperbolic metamaterials with magnetic control," *Appl. Phys. Lett.* **100**(16), 161108 (2012).
18. H. C. van de Hulst, *Light Scattering by Small Particles*, Dover, New York (1981).
19. P. Wang et al., "Analysis of light extraction efficiency of GaN-based light-emitting diodes," *J. Phys. Conf. Series* **276**(1), 012083 (2011).
20. V. Karagodsky, F. G. Sedgwick, and C. J. Chang-Hasnain, "Theoretical analysis of sub-wavelength high contrast grating reflectors," *Opt. Express* **18**(16), 16973–16988 (2010).
21. E. D. Palik, *Handbook of Optical Constants of Solids*, Academic Press, San Diego (1985).

Biographies and photographs of the authors not available.